were used for detection of neutrons. The detectors were placed at different polar and azimuthal angles in a geodesic dome structure of the National Array of Neutron Detectors (NAND) [1]. Each detector was at a distance of 175 cm from the target. Fission fragments were detected using two large area (20 cm × 10 cm) position sensitive multi-wire proportional counters (MWPCs), placed at a folding angle of 154°. The forward detector was kept at 40° (27 cm from the target) and the backward detector was placed at 114° (24 cm from the target). The arrangement is shown in Fig 5.1.15.1. The MWPCs were operated with iso-butane gas at ~ 4mbar.

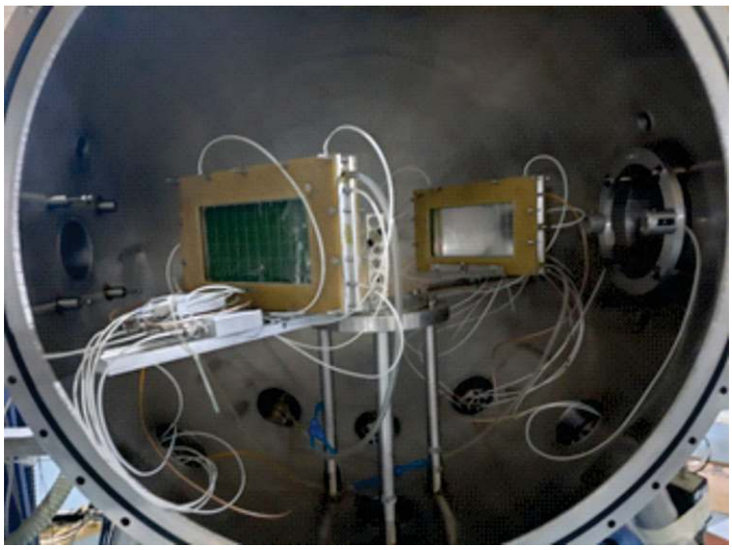

Fig. 5.1.15.1: Experimental setup with two MWPCs placed at 154° folding angle and two Passivated Implanted Planar Silicon (PIPS) detectors at 15° with respect to the beam direction.

The trigger for the data acquisition system was generated by logical OR of the two timing signals (from anodes of the two MWPCs) which was further AND-gated with the RF of the beam. The trigger was delayed with respect to neutron detectors and MWPC signals to generate a COMMON STOP mode within a TDC range of 400 ns. Data were acquired with NiasMars (Multi-parameter Acquisition Root-based Storage) software. Analysis of data is being performed with the ROOT package [2] which is an open-source data analysis framework. Detailed analysis is in progress.

REFERENCES

[1] P. Sugathan *et al.*, Pramana – J. Phys. **83**, 807 (2014).

[2] https://root.cern.ch/

5.1.16 Spectroscopic study of ^{40}K

Rozina Rahaman[1], Abhijit Bisoi[1], Y. Sapkota[1], Ananya Das[1], A. Gupta[1], S. Ray[2], S. Sarkar[1], Yashraj[3], A. Sharma[4], Bharti Rohilla[5], I. Ahmed[3], K. Katre[3], S. Dutt[3], S. Kumar[3], Gururaj[3], R. P. Singh[3], Rakesh Kumar[3] and S. Muralithar[3]

[1]*Indian Institute of Engineering Science and Technology, Shibpur, Howrah 711103, India*

[2]*Amity Institute of Nuclear Science and Technology, Noida, Uttar Pradesh 201313, India*

[3]*Inter-University Accelerator Centre, New Delhi 110067, India*

[4]*Department of Physics, Himachal Pradesh University, Shimla, Himachal Pradesh 171005, India*

[5]*Department of Physics, Panjab University, Chandigarh 160014, India*

The *sd-pf* interface nuclei usually exhibit the characteristic of spherical single-particle excitation spectra and their spectra are well explained by the spherical shell-model [1]. Using the sophisticated detectors and advanced data acquisition systems, it is now possible to study these nuclei at higher angular momentum and excitation energy. As a result, the coexistence of single-particle and collective excitations have been observed in a few *sd-pf* interface nuclei *viz*., ^{40}Ca [2], etc. In most of the cases, single-particle nature is dominated at lower excitation energies whereas collective excitations in terms of normal deformed or even super-deformed (SD) bands are observed at relatively higher excitation energies. Shell-model calculations with multi-particle multi-hole excitation have been performed successfully to understand the microscopic origin of these observed SD bands.

^{40}K is the isobaric partner of ^{40}Ca. So, we may also expect collective excitations at higher excitation energy in ^{40}K, generated from multi-particle multi-hole excitations. ^{40}K was previously studied by Soderstrom *et al*. [3] through heavy-ion reaction. Several states with excitation energy up to 8 MeV and spin up to 10$^-$ were discovered. The authors assigned the spin and parity of these levels tentatively, based on the comparison of the branching ratios to the Weisskopf value. Therefore, our primary motivation was to investigate the high-spin structure of ^{40}K and search for collective excitation in ^{40}K.

High-spin states in ^{40}K were populated through the ^{19}F(^{27}Al, αnp)^{40}K reaction at 68 MeV. The ^{19}F beam was provided by the 15UD Pelletron accelerator at IUAC. The target was ^{27}Al (0.43 mg/cm^2) evaporated on 11.4 mg/cm^2 Au backing which was fabricated at the Target Laboratory of IUAC. We used a diffusion pump based thin film coating unit for target preparation. A multi-detector array (Indian National Gamma Array (INGA)), comprising of 12 Compton-suppressed Clovers, was used to detect the γ-rays. These twelve Clovers were mounted at four different angles *viz.*, 148° (4), 90° (4), 57° (1) and 32°(3) with respect to the beam axis. The data sorting program NiasMARS, developed by IUAC, was used to generate angle-independent symmetric and angle dependent E_γ- $E_\gamma$matrices, which were then analyzed by the sorting program INGASORT [4]. We used a few online γ-lines ranging from 300 to 4000 keV for energy calibration of the Clovers. The relative efficiency calibrations of the Clovers were performed using ^{152}Eu and ^{66}Ga radioactive sources. The ^{66}Ga source having γ-energy 833 to 4806 keV was prepared through ^{19}F(^{51}V, 3np)^{66}Ga reaction at 68 MeV in the same experimental setup.

In ^{40}K, we found a few new levels and transitions. We have placed them in the level scheme based on their coincidence relationship and measured relative intensities. In order to assign the spin and parity of these levels, DCO (directional correlation of γ-rays emitted from excited states) and polarization measurements will be carried out. Lineshape analysis will be performed to extract the lifetime of the levels. Large basis shell model calculation with multi particle-multi hole excitations will be carried out to understand the microscopic origin of these levels.

REFERENCES

[1] http://www.nndc.bnl.gov.

[2] E. Ideguchi *et al.*, Phys. Rev. Lett. **87**, 222501 (2001); C. J. Chiara, E. Ideguchi, M. Devlin, D. R. LaFosse *et al.*, Phys. Rev. C **67**, 041303(R) (2003).

[3] P. -A. Soderstrom *et al.*, Phys. Rev. C **86**, 054320 (2012).

[4] R. K. Bhowmick *et al.*, Proc. DAE-BRNS Symp. Nucl. Phys. **B44**, 422 (2001).

5.1.17 Evaporation residue cross section measurements for ^{30}Si+^{176}Yb and ^{19}F+^{187}Re reactions

Hajara K.[1], M. M. Musthafa[1], N. Madhavan[2], S. Nath[2], J. Gehlot[2], Gonika[2], Midhun C. V.[1], Shaima Akbar[1], F. S. Shana[3], Muhammad Shan P. T[1], Amninder Kaur[4] and Rohan Biswas[2]

[1]*Department of Physics, University of calicut, Kerala 673635 India*

[2]Inter-University Accelerator Center, Aruna Asaf Ali Marge, New Delhi 110067, *India*

[3]*Department of Physics, Govt. Arts and Science College, Calicut 673018, India*

[4]*Department of Physics, Panjab University, Chandigarh 160014, India*

In order to investigate the entrance channel dependence of quasifission, evaporation residue (ER) cross section (σ_{ER}) measurements were carried out for the systems ^{30}Si+^{176}Yb and ^{19}F+^{187}Re. The measurements were performed using the HYbrid Recoil mass Analyzer (HYRA) at IUAC. The measured cross sections were compared with another system *viz.*, ^{12}C+^{194}Pt populating the same compound nucleus (CN) ^{206}Po. The entrance channel parameters such as charge product, mass asymmetry, deformation of the target nuclei, isospin asymmetry in the entrance channel and effective fissility were studied. The excitation functions for the two reactions ^{19}F+^{187}Re and ^{30}Si+^{176}Yb are compared with the corresponding statistical model predictions in Fig. 5.1.17.1 and Fig. 5.1.17.2, respectively.

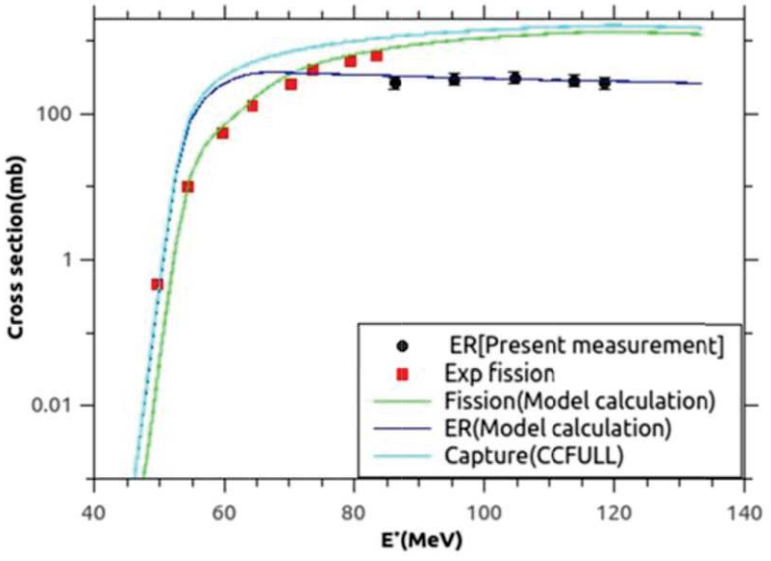

Fig. 5.1.17.1: Measured ER cross sections for the reaction ^{19}F+^{187}Re along with the statistical model and coupled-channels calculation. Fission data are taken from Ref. [2].

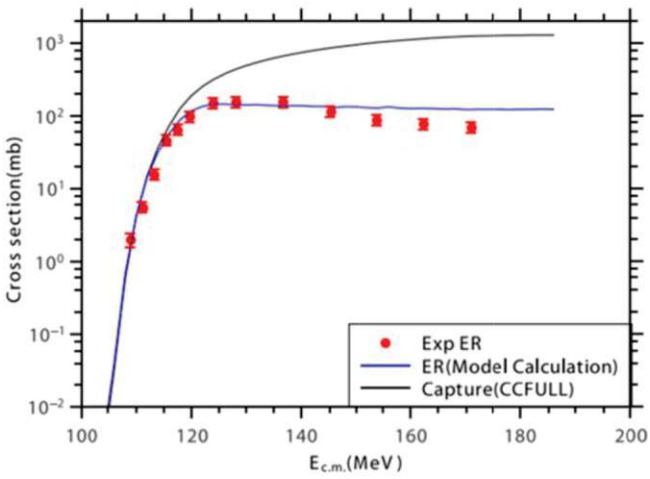

Fig. 5.1.17.2: Measured ER cross sections for the reaction ^{30}Si+^{176}Yb along with the statistical model and coupled-channels calculation.

By comparing the measured cross sections with the statistical model calculations, marked reduction in the cross sections is observed for the ^{30}Si-induced reaction. This reduction in the cross sections is attributed to the presence of quasifission for this reaction. On the other hand, the cross sections measured for the ^{19}F-induced reaction are in good agreement with the statistical model calculations. This implies that there is no effect of any non-compound nuclear processes in this reaction.

To explore the entrance channel dependence of quasifission, the reduced ER cross sections for these systems are compared with the same for ^{12}C+^{194}Pt [1]. Energy and cross sections are transformed as E → ε and $\sigma_{ER} \rightarrow \Sigma_{ER}$:

$\epsilon = \frac{E-V_B}{\hbar\omega}$ and $\Sigma_{ER} = \sigma\left[\frac{2E}{\hbar\omega R_B^2}\right]$.

Here, the potential barrier is fitted with a parabola with V_B, the barrier height located at $R_B$and curvature parameterħωwhere R_B is the fusion radius. The reduced ER cross sections for the three systems are plotted in Fig. 5.1.17.3.

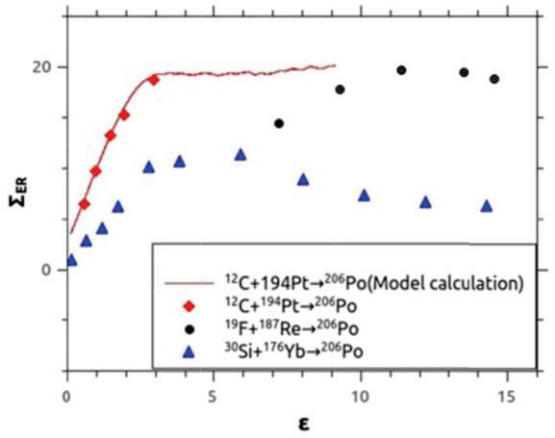

Fig. 5.1.17.3: The reduced ER cross sections for three reactions.

For ^{12}C+^{194}Pt, entrance channel mass asymmetry α = 0. 883 which is greater than α_{BG} , the Businaro-Gallone mass asymmetry (α_{BG} = 0.846). Hence the driving force due to the nuclear potential favours a compact CN with high survival probability. However, for mass symmetric reactions, for which α = 0.706, which is less than α_{BG}, the system breaks without forming a completely equilibrated CN. The comparison also shows clear dependence of quasifission on entrance channel charge product (Z_pZ_t). Earlier dynamical models predicted the onset of quasi fission for very heavy systems with the Coulomb factor $Z_pZ_t > 1600$, where Z_p and Z_t are the atomic numbers of the projectile and the target, respectively. However, quasifission was reported in many asymmetric reactions using deformed targets at sub- and near-barrier energies, even though the Z_pZ_t values were much lower than 1600. The fusion hindrance can also be observed in terms of the static deformation of the target nucleus and also the orientation of the colliding nuclei. The static deformation *(β_2 = 0.289)* is more for ^{176} Yb than ^{194} Pt *(β_2 = 0.13)* and hence the elongated configuration favours non-compound fission.

REFERENCES:

[1] A. Shrivastava *et al.*, Phys. Rev. Lett. **82**, 699 (1999).

[2] Tathagata Banerjee and S. Nath et al., Phys. Rev. C **96**, 014618 (2017).

5.2 MATERIALS SCIENCE

Ambuj Tripathi

The materials science facilities support a large number of research programmes of users from universities and institutions from all over India and are also providing critical support in many programmes of national importance from various organizations. among other. This year there were a total of 28 user experiments spread over 108 shifts. The experiments were performed without any major facility break down in materials science beamlines facilities leading to beam time loss. The experiments included 17 BTA runs spread over 61 shifts, associated with students' Ph.D. programmes and this year priority was given to senior scholars in fifth year of Ph.D. The swift heavy ion (SHI) irradiation experiments mostly utilize irradiation facilities in materials science beamlines in beamhall-I. However, three special runs from URSC Bangalore, SAC Ahmedabad and SCL involving low fluence irradiation was performed in the GPSC. Besides irradiation facilities, materials science group is also providing support to users with many materials synthesis and characterization facilities while keeping Covid protocols in place. The materials science research programmes are being carried out in a wide range of energies varying from tens of keV to hundreds of MeVand a list of publications is given in section 6. The Materials Science group webpage in IUAC website was recently updated and detailed information about activities and facilities is available there. This year there were many interesting results in the various areas of research including those on radiation stability of devices, sequential implantation, bandgap tuning, nanostructuring, nanocomposites and applications and some of these are highlighted below.

Swift heavy ions from Pelletron are widely used for user experiments. The radiation stability of BJT transistors, which are important in silicon integrated circuits fabricated in bipolar and bipolar complementary metal oxide semiconductor (BiCMOS) processes were studied using 80 MeV N^{6+} and 100 MeV P^{7+} ions utilizing in-situ electrical measurement facility. Similarly 50 MeV Lithium ion irradiation studies on 200GHz SiGe HBTs at 150K and 300K with ion dose range from 1 to 30 Mrad showed that both forward and inverse excess base currents increased after lithium ion irradiation at both temperatures and forward DI_B of HBTs irradiated at 300K increased around three orders of magnitude. With the aim of tailoring the multiferroic as wells as RRAM mechanism, the BSFO/CFO/LNO devices were irradiated with 150 MeV Ag ions and it is shown that point defects at the interface of the antiferromagnetic BSFO and ferromagnetic CFO modifies the magneto-transport of the devices. The electronic excitations, induced by 125 MeV Ag ions show a variety of emissions through bound states of O vacancies and implanted N ions and are used for bandgap tuning in SrTiO3 films in the range of 2.93-3.78 eV. To study the temperature dependent irradiation induced effect zirconolite compositions with the doping of simulated oxides, samples were irradiated with 120 MeV Au^{9+} ions at a fluence $3E^{13}$ ion/cm^2 at different temperatures 800K, 900K and 1000 K. Bulk and Ga- doped Al_2O_3 thin-films, were irradiated with 100MeV Ag^{9+} ions with ion fluence of 1×10^{11} ions/cm^2, to 1×10^{13} ions/cm^2 and a transformation from a metal- like behavior (low-temperature region) to a semiconductor-like (high-temperature region) behavior was observed. Some of the other important studies include, the effects of swift heavy ion (SHI) irradiation on the structural, optical, electrical and magnetic properties of Ca-doped $BiFeO_3$/$LaNiO$/$LaAlO_3$ heterostructures, study of 120 MeV Ag ion-induced effect on $Co_{0.5}Cu_{0.5}Fe_2O_4$/polypyrrole nanocomposites with potential applications in transformer cores in the microwave region etc. The anisotropic magnetodielectric measurements were carried out in polycrystalline LCMO and LSMO after irradiation with Ag^{+15} ions at an ion fluence of 1×10^{11} ions/cm^2, to 1×10^{13} ions/cm. The crystalline KNN films were irradiated with 120 MeV Au ion beam and enhanced PL of irradiated KNN samples with ion fluence and the TRPL results show the reduction of non-radiative recombination centers after ion beam irradiation. ZnO thin films irradiated with 50 MeV Ni and 120 MeV Au ions for tuning of visible photolumuniscence. Interface modification of Fe/Cr/Al magnetic multilayer by Swift Heavy Ion Irradiation is studied and its shown that longer spike duration in thinner film results in higher mixing. The electronic excitation-induced disorder engineering in the $Gd_2Zr_2O_7$ system on irradiation of 100 MeV I^{7+} ions observed that superstructure reflection disappeared with the enhanced fluence, which indicates pyrochlore to defect fluorite structure phase transformation. It is demonstrated that that by selecting appropriate amount of doping, fluence and energy during SHI irradiation, it is possible to alter the characteristics of BiFeO3 films such as I-V and energy band gap, with potential device applications.

Besides Pelletron accelerator, ion beams from low energy ion beam facilities: LEIBF and NIBF are also widely used. It has been shown that optimized $SrSO_4$:Eu nanophosphor when compared with commercially available standard TLD-100 (LiF:Mg,Ti) shows 12.5 times higher sensitivity. Growth of low resistive nickel mono-silicide phase under low energy Si ion irradiation at room temperature is investigated after irradiation with 120 keV Si ions with fluences varying from $7 \times 10^{14}$to 7×10^{15} ions-cm^{-2} at room temperature. Structural and phase transformation studies of 1.4 MeV Kr ion beam irradiated zirconia thin films was studied and it is observed that increasing fluence resulted the evolution of a cubic phase. Implantation with Au and Cu ions with 80 keV and 140 keV energy respectively for enhancing light harvesting and minimal recombinations in TiO_2 NP-NF and TiO_2 NP- MXene based photoelectrodes is studied. Surface Plasmon Resonance (SPR) properties of bimetallic nanoparticles with applications in plasmonic sensors are taken up with sequential implantation with 80 keV Au^- ions, (2.4×10^{16} ions/cm^2) and then with 65 keV Ag^- ions, (6×10^{15} ions/cm^2) respectively using negative ion implanter facility. Ion implantation studies on Ga_2O_3 are initiated after implantation with Ge and Si ions for the fluences ranging from 10^{13} to 10^{15} cm^{-2}. using NIBFfacility. Thin films of HfO_2 (on both p- and n- silicon substrate) prepared by ALD were irradiated with Ar, Ne, Kr and Xe ions using ion fluence of 5×10^{16} ions/cm^2 from LEIBF with aim of tailoring of hafnium oxide as a material for non-volatile memory. The effect of low energy ion irradiation with Ar beam having 120 keV energy has been investigated on transparent ZnO thin films to study the modifications in structural and optical properties of ZnO. Gamma irradiation induced modifications are also studied. The gamma irradiation effects on the structural, optical, electrical and shielding properties of lithium borate glasses showed an increase in activation energy of LBO glasses from~ 0.13 eV to ~0.42 eV for glasses irradiated at 100 kGy and is explained on the basis of hopping mechanism in the glass matrix . The structural and optical properties of RF sputtering deposited zirconium oxide (ZrO_2) thin films have been modified using high dose gamma irradiation. Some of the other studies initiated include demonstration of pinning-assisted out-of-plane anisotropy in reverse stack FeCo/FePt intermetallic bilayers for controlled switching in spintronics, synthesis and diverse property studies on RGO based Ni-doped Cobalt oxide nanomaterials etc. In the search for magneto-electric properties in corundum structured metal oxides for applications in low power spintronic devices, studies have been initiated on Hematite (α- Fe_2O_3) as the basic system and enhanced electrical conductivity by doping tetravalent elements such as Si, Ge and Sn. Further studies on synthesis of silver nanoparticles and their use as SERS substrate in chemical and biological sensing and effect of beam line are currently in progress.

Efforts in organizing workshops, schools and conferences on specialized topics continued this year so that the users are familiar with state of art experiments and facilities. Due to COVID situation the activities were undertaken in an online mode. 6th International Conference on Nanostructuring with Ion Beamss (Oct 5-8, 2021), Online school/workshop on Ion Beams in Sensors and Developments (Sept 7-8, 2021) and Virtual School on Microscopic Techniques (Nov 9-12, 2021) were organized this year and details are given in section 6.

5.2.1 Gamma irradiation induced effects on the structural, optical, electrical and shielding properties of lithium borate glasses

S Karthika[1], K Asokan[2], RC Meena[2], I Sulania[2], K Marimuthu[3], S Shanmuga Sundari[1*]

[1]*Department of Physics, PSGR Krishnammal College for Women, Coimbatore, 641004, India*
[2]*Materials Science Division, Inter University Accelerator Centre, New Delhi, 110067, India*
[3]*Department of Physics, Gandhigram Rural University, Gandhigram, 624302, India*

Lithium borate glass of composition $25Li_2O.75B_2O_3$ were prepared using melt quenching technique. The changes in their structural, optical and electrical parameters due to gamma irradiation was investigated and its shielding ability was discussed. Lithium carbonate and boric acid were melted at 950 ºC for 2 hours to assure complete homogenous melt and quenched in a stainless-steel mould that was preheated to 300 ºC. The glasses were annealed at 310 ºC for 6

hours to increase its thermal stability. The prepared glasses were transparent, colorless and inclusion free. The glasses were irradiated at dose of 2.906 kGy per hour for 20, 40, 60, 80 and 100 kGy using a ^{60}Co gamma source from a Gamma chamber 1200 manufactured by Board of Radiation Isotope Technology (BRIT), at IUAC New Delhi. As the radiation dose increases color centers were formed in the prepared glasses, for higher dosages the glasses turned to be black and are shown in figure 1. The structural changes were carried out using XRD facility at IUAC, New Delhi and FTIR at Avinashilingam Deemed University, Coimbatore. XRD confirms amorphous nature of glass which is found to be unaltered even for high dosage of gamma irradiation. The theoretical structural parameters such as density, optical basicity, ionicity, boron-boron separation, bond density, molar volume and oxygen packing density were also calculated. FTIR shows the breakage of bonds due to gamma irradiation. Borates possess BO_4 and BO_3 units, due to gamma irradiation, there is destruction in BO_4 and formation of BO_3 units. The theoretical structural parameters such as density, optical basicity, ionicity, boron-boron separation, bond density, molar volume and oxygen packing density were also calculated. The optical absorption spectra of the prepared glasses were recorded using the HITACHI U-3300 UV-VIS spectrophotometer at IUAC New Delhi in UV-visible range of 200–800 nm. The direct band gap of pristine and gamma irradiated LBO glasses were calculated from absorption data using Tauc's plot [1] and is found to vary from 3.74 to 3.49 eV. The results showed that direct band gap values decreased with the increasing gamma irradiation [2]. The dielectric spectroscopy and A.C. conductivity mechanism of the glasses was analyzed using LCR meter at PSGR Krishnammal College for Women, Coimbatore. The conduction mechanism in the glasses were studied from room temperature to 423 K at the frequency range of 1 kHz to 3 MHz. The activation energy of the glasses was calculated before and after gamma irradiation using Arrhenius plot [3]. High doses of gamma irradiation resulted in an increase in activation energy of LBO glasses from 0.1269 eV for unirradiated to 0.4213 eV for glasses irradiated at 100 kGy as a function of frequency. This increase is due to hoping mechanism in the glass matrix [4]. These changes in structural, optical and electrical properties are due to radiation induced defects in the prepared glasses. The shielding ability of the prepared glass samples were estimated using theoretical simulations by PhyX- PSD software.

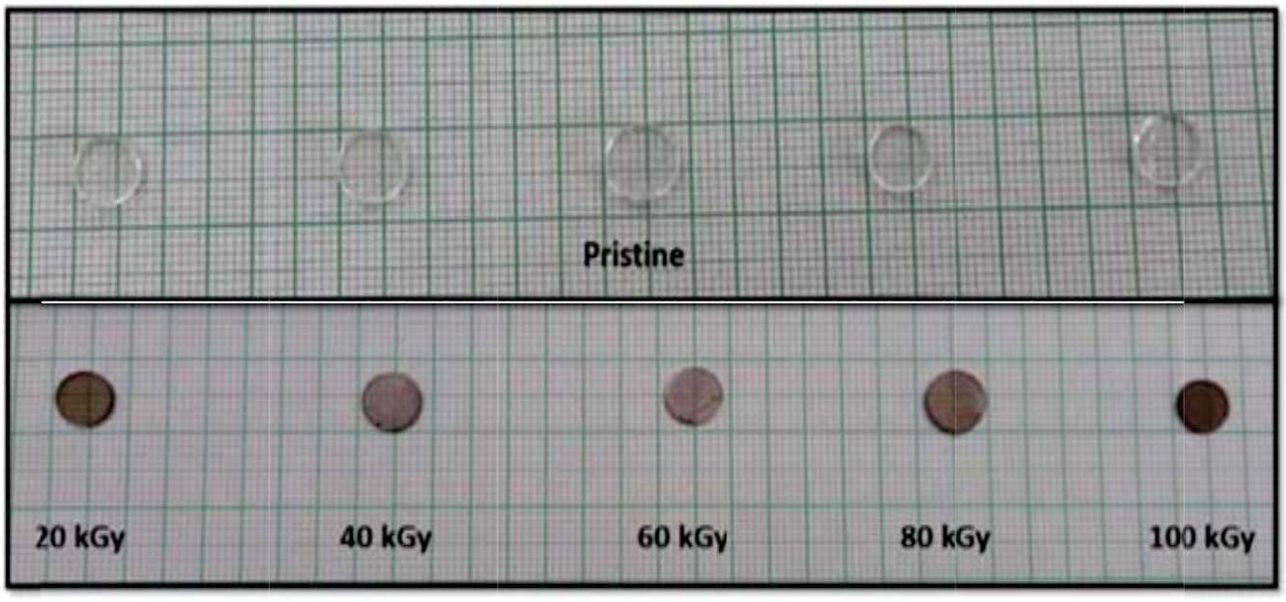

Figure 1. The pristine and gamma irradiated LBO glasses.

REFERENCES

[1] A.M Fayad, W.M. Abd-Allah, F.A. Moustafa, Effect of Gamma Irradiation on Structural and Optical Investigations of Borosilicate Glass Doped Yttrium Oxide. Silicon 799–809. 10(2018)

[2] N.A. El-Alaily, R.M Mohamed, Effect of irradiation on some optical properties and density of lithium borate glass, Materials Science and Engineering: B, Volume **98**, 193-203, Issue 3(2003).

[3] N.A. El-Alaily, R.M. Mohamed, "Effects of fast neutron and gamma irradiation on electrical conductivity of some borate glasses", Journal of Nuclear Materials Volume **303**, Issue 1, 44-51(2002).

[4] A. S. Das and D. Biswas, "Investigation of AC conductivity mechanism and dielectric relaxation of semiconducting neodymium-vanadate: temperature and frequency dependency," Materials Research Express Volume **6**, Issue 7, 075206(2019).

5.2.2 Growth of low resistive nickel mono-silicide phase under low energy Si ion irradiation at room temperature

G Maity[1], S. Ojha[2], G.R. Umapathy[2], Shiv P. Patel[1], Anter El Azab[3], Kailash Pandey[4], Santosh Dubey[4*]

[1]*Department of Pure and Applied Physics, Guru Ghasidas Vishwavidyalaya (A Central University), Bilaspur 495009, India*

[2]*Inter University Accelerator Centre, Aruna Asaf Ali Marg, New Delhi 110067, India*

[3]*Materials Engineering, Purdue University, West Lafayette 47907, United States*

[4]*Department of Physics, School of Engineering, University of Petroleum and energy studies, Dehradun, India*

Nickel mono-silicide (NiSi) is considered as a promising material for developing low resistance contacts in complementary metal-oxide-semiconductor technology. In the present work, we report the effect of Ni film thickness on orientation control of low resistive Nickel mono-silicide (NiSi) phase formation using low energy ion irradiation at room temperature. In order to study the effect of Ni film thickness on NiSi phase formation, the Ni films of thicknesses 30 nm and 60 nm were deposited on Si (111) substrate using thermal evaporation technique in a high vacuum chamber. The as prepared Ni/Si samples were then irradiated via 120 keV Si ions with different fluences of 7×10^{14}, 1×10^{15}, 3×10^{15} and 7×10^{15} ions-cm^{-2} at room temperature. The x-ray diffraction and transmission electron microscopy measurements clearly confirm the formation of mono-silicide phase. The composition of the NiSi phase is determined by Rutherford backscattering spectrometry measurements. The crystallinity of NiSi phase has been observed to be better for 60 nm Ni film as compared to the 30 nm Ni film on Si substrate. Most of the NiSi crystallites are found to be oriented in (103) lattice plane. The resistivity and sheet resistance of the NiSi/Si films are found to be very low. The role of composition of Ni and Si in NiSi phase on resistivity and sheet resistance of the films has been investigated carefully. The detailed mechanisms behind the above observations have been discussed in the paper.

Corresponding author: santosh.dubey@ddn.upes.ac.in

REFERENCES

[1] G Maity, S. Ojha, G.R. Umapathy, Shiv P. Patel, Anter E1 Azab, Kailash Pandey and Santosh Debey, Mater. Res. Express **5,** 065506(2018)

5.2.3 Elevated Transition Temperature of VO_2 Thin Films via Cr doping

M. Zzaman[1,2], R. Dawn[1], J. B. Franklin[3], A. Kumari[1], V. K. Verma[4], R. Shahid[2], U. K. Goutam[5], K. Kumar[6], R. Meena[7], K. Asokan[7,8], and V. R. Singh[1]*

[1]*SpinTec Laboratory, Department of Physics, Central University of South Bihar, Gaya 824236, India*[2]*Department of Physics, Jamia Millia Islamia (Central University), New Delhi-110025, India*

[3]*Department of Energy Storage and Distribution Resources, Lawrence Berkeley National Laboratory, Berkeley, CA 94720, USA*

[4]*Department of Physics, Madanapalle Institute of Technology & Science, Angallu, Madanapalle -517325, India*

[5]*Technical Physics Division, Bhabha Atomic Research Centre, Trombay, Mumbai- 400 085, India*

[6]*Department of Physics, Ranchi University, Ranchi 834008, India*

[7]*Materials Science Division, Inter-University Accelerator Centre, Aruna Asaf Ali Marg, New Delhi 110067, India*

[8]*Department of Physics & Centre for Interdisciplinary Research, University of Petroleum and Energy Studies (UPES) Dehradun, Uttarakhand 248007 India*

A KrF excimer laser ($\lambda = 248$ nm, repetition rate of 5Hz and pulse energy of 210 mJ) with a fluence of 1.1 J/cm^2 was focused onto $V_{1-x}Cr_xO_2$ (x = 0-30%). An ultrasonically cleaned r-cut sapphire substrate was kept at a certain temperature during the growth of the films. The depositions were carried out in an oxygen atmosphere at a partial pressure of about 10 m Torr. The Hall Effect test was performed for transport properties utilizing a magnetic field of 0.5 T at R.T to estimate carrier density and resistivity using the Ecopia Hall effect measurement system, HMS-3000.

The I-V measurements were performed on our as-prepared films to understand the electrical transport properties. The data from these measurements are summed up in Table 1. The results showed an enhanced conductivity by 15 times with an increase in Cr concentration from 0 to 30%. This remarkable increase in conductivity is further complemented by the charge carrier concentration in the films where the concentration increased enormously by 5 times with just 5% Cr in the matrix than with pristine films. Astonishingly with 30% Cr in the matrix, the carrier concentration increased by whopping 433 times than pristine films and thereby could be the possible factor for the enhancement of conductivity. In contrast to these two results, we see a remarkable reduction in mobility inside our films by a factor of 20. This brings the film in a highly conducting semiconductors range. In addition to that Hall coefficient value also decreased from 3.29 cm^3/C for the pristine film to 0.01 cm^3/C for the highest doped films. This has to be the case as the Hall coefficient is inversely proportional to carrier concentration. Thus, an increase in concentration will result in a decrease in the Hall coefficient. Thus, our results are in accord with each other and